applied sciences

MDPI

Article

DEM-Based Traversability Map Generation for 2.5D Autonomous Multirobot Navigation

David Orbea *, Juan Mateos Budiño, Christyan Cruz Ulloa, Jaime del Cerro and Antonio Barrientos *

Centro de Automática y Robótica (UPM-CSIC), Universidad Politécnica de Madrid-Consejo Superior de Investigaciones Científicas, 28006 Madrid, Spain; j.cerro@upm.es (J.d.C.)
* Correspondence: david.orbea@upm.es (D.O.); antonio.barrientos@upm.es (A.B.)

Abstract

Autonomous mobile robots operating in outdoor environments must have an understanding of the surrounding terrain geometry to ensure efficient and safe navigation. This article presents a DEM-based intelligent traversability mapping framework to transform open-source geospatial data into slope-aware cost maps for multirobot autonomous navigation within the ROS2 framework. The proposed cv_gdal algorithm automatically processes GeoTIFF elevation data using adaptive slope thresholding based on each robot's physical capabilities, generating ROS-compatible cell occupancy maps. Six regions of Spain were used to evaluate terrain representation accuracy and navigation performance in kilometer-scale DEMS. This framework enables autonomous perception-to-planning pipelines and supports the deployment of multirobot systems for search and rescue (SAR) tasks. By bridging geospatial analytics with robotic perception and adaptive decision-making, this work contributes to the development of intelligent, self-configuring robotic systems capable of operating safely in complex outdoor environments.

Keywords: intelligent navigation; DEM; traversability mapping; autonomous perception; ROS2; multirobot systems; SAR

1. Introduction

The evolution of intelligent robotic systems is transforming the way autonomous agents perceive and interact in complex environments. For outdoor applications such as Search and Rescue (SAR), agriculture, and environmental inspection, ground robots must be able to autonomously interpret terrain conditions, ensure traversability, and plan safe trajectories. These capabilities represent the convergence of perception, decision-making, and adaptive control, which are essential principles of intelligent robots.

Among the variables related to mobility, terrain geometry is one of the most critical, as variations in slope, roughness, and elevation directly affect the robot's stability, energy consumption, and mission reliability. Existing approaches often lack a unified framework to transform raw geospatial data into representations tailored to a robot's physical capabilities.

Traditional systems rely on computer vision or LiDAR systems to generate cell occupancy maps, which lack the global contextual awareness essential for large-scale missions. In this regard, digital elevation models (DEMs), which are rasterized height maps derived from satellite and geospatial data, are a scalable alternative for representing outdoor environments. When processed correctly, they are useful for static terrain representation and as sources for semantic analysis used for robot navigation.

Academic Editors: Qiang Liu and Alessandro Gasparetto

Received: 9 January 2026
Revised: 19 March 2026
Accepted: 20 March 2026
Published: 30 March 2026

This study proposes an intelligent traversability system based on DEMs to transform elevation data into cost maps with slope information, applied to the autonomous navigation of multiple robots in the Robot Operating System (ROS2) environment. The core of this system is the algorithm "cv_gdal", which integrates geospatial image processing libraries (GDAL, OpenCV, and QGIS) to analyze elevation gradients, apply specific slope thresholds for each robotic platform, and generate ROS2-compatible occupancy maps without user intervention. Thus, the system allows individual robots to interpret the environment according to their physical capabilities, achieving adaptive and decentralized mission planning, which constitutes a novel contribution as a fully automated DEM-to-ROS2 pipeline framework designed for multirobot systems.

This work is part of the Collaborative Search and Rescue (CESAR) project developed by the Robotics and Cybernetics Group (ROBCIB) at the Polytechnic University of Madrid (UPM-CSIC). In this project, a fleet of Unmanned Ground Vehicles (UGVs) autonomously deploy a Cable-Actuated Parallel Mobile Robot (CAMP) into sinkholes for exploration, inspection, and victim search tasks. The methodology presented offers the high-level terrain intelligence required for multi-robot operations, bridging global geospatial data with local robotic perception, providing a tool for systematic evaluation of terrain-based navigation strategies before field deployment.

The proposed framework aligns with recent trends in intelligent perception and adaptive navigation, where mapping is treated as a reasoning process rather than a static geometry task. By combining DEM processing, slope-based traversability analysis, and ROS2 multi-agent integration, this work contributes to the development and deployment of autonomous systems capable of configuring their navigation environment using information from geospatial data sources. In addition to its contribution to SAR missions, this approach is applicable to transportation planning, agricultural robotics, and planetary exploration, where autonomous terrain interpretation has a significant impact.

Terrain information extracted from GeoTIFF via DEM slope processing is shown in Figure 1, which is subsequently adapted to the physical constraints of the robot through configured parameters such as the robot footprint, inflation radius, and kinematic limits, defined in the Nav2 configuration. These global and local cost maps based on elevation and slope maps allow the estimation of minimum path width, safe clearance margins, and suitability of the surface for motion. This integration ensures that the traversable map produced from the digital terrain data yields path candidates that are physically feasible for the actual robot and compatible with ROS2 simulation.

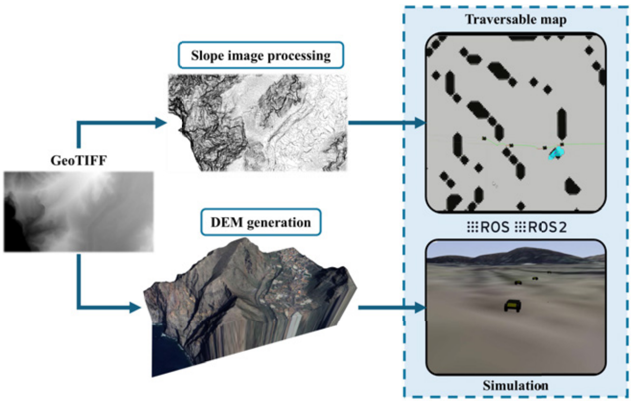

Figure 1. Proposed methodology overview. Source: Authors.

As a preamble to this article, a detailed description of the configuration, phases, and mission tasks of the robotic fleet is given in [1].

The article is structured as follows: Section 2 presents a review of the state of the art and related previous work; Section 3 describes the methodology used, detailing the cv_gdal algorithm, the terrain processing workflow, and its integration into ROS2; Section 4 presents the results obtained; and finally, Section 5 presents the conclusions with directions for future work on learning-based terrain reasoning and real-world deployment.

2. Related Work

Grasping terrain structure and assessing navigability continue to be key difficulties for smart robotic systems operating in outdoor and irregular settings. Initial studies on DEM-based terrain representation identified geometric indicators such as slope, curvature, and roughness as the basis for evaluating traversability. Ref. [2] presented a rule-based approach to interpreting elevation maps to assess mobility, while ref. [3] conducted an extensive review of terrain analysis methods for unmanned ground vehicles (UGVs). The extensive accessibility of open-access geospatial datasets, airborne LiDAR surveys, and satellite-based elevation models [4] has since facilitated large-scale environmental modeling for robot navigation.

Recent studies utilize modern DEM fusion and improvement techniques, incorporating deep-learning super-resolution methods to refine elevation maps [5,6]. Currently, the study of traversability applied in mobile robotics is based on sophisticated methods of perception, artificial vision, and intelligent control.

As ref. [7] highlights, understanding terrain is vital for mobile robot navigation in unstructured environments. In this context, 2.5D raster-based terrain modeling has been proven to be effective in modifying locomotion strategies and identifying irregular terrain. Unlike full 3D volumetric representations, which encode multi layer structures, a 2.5D model stores a single elevation value per coordinate (x,y), creating a continuous height field that includes slopes, depressions, and surface variations with low computational cost, making this terrain representation suitable for UGVs, where locomotion decisions depend more on terrain shape than volumetric detail.

The application of aerial and satellite imagery to create navigation maps in ground robotics has been addressed in recent years. Ref. [8] illustrated the application of processed terrain images for occupancy-grid-based navigation in outdoor logistics, while refs. [9,10] investigated the combination of multi-source satellite and low-orbit imagery through deep learning to generate base maps for unmanned ground vehicle navigation. Ref. [11] evaluated elevation-based maps alongside UAV-created photogrammetric models, confirming the effectiveness of geospatial tools to produce 3D reconstructions and traversability maps relevant to terrestrial robotics.

In the field of robotics, traversability mapping has traditionally relied on geometric metrics such as slopes, local gradients, or roughness thresholds [12–14]. Nevertheless, the emergence of smart perception has sparked the incorporation of learning-based techniques for terrain evaluation. Visual terrain classification using CNNs has been shown to generalize effectively in varying environments [15], while deep learning models such as TerrainNet [16] have exhibited impressive results in unstructured environments. Ref. [6] developed a deep-learning traversability estimator that uses geometric characteristics and recent robot movement, tested in both simulations and real UGV systems.

Recent approaches have also focused on creating slope-aware maps that can be integrated with robotic systems. Ref. [17] assessed traditional computation methods along with DEM-based techniques to generate slope maps in ROS2, finding that DEM computation provides greater efficiency in static and dynamic settings. Similarly, ref. [18] suggested a combined 2D to 2.5D elevation-map fusion method to create traversability maps while taking safety constraints into account in path planning.

https://doi.org/10.3390/app16073351

Autonomous navigation remains largely dependent on sampling-based planners due to their ability to scale in expansive natural landscapes. Traditional algorithms like Rapidly exploring Random Trees (RRT), RRT* (RRT-Star), Probabilistic Road Maps (PRM), and Batch Informed Trees (BIT) continue to be essential, while subsequent improvements include terrain-awareness through slope limitations, risk assessments, or uncertainty modeling [19,20]. However, these planners typically presume the availability of preprocessed costmaps and rarely consider the entire perception-to-planning workflow—from raw DEM ingestion to the creation of ROS2-compatible costmaps—especially when dealing with kilometer-scale settings.

Navigation using satellites and map extraction has also been investigated for UGV navigation. Ref. [5] used CNN-driven segmentation of georeferenced satellite images to create traversable paths for ground robots. Ref. [21] introduced OS-RFODG, an open-source ROS2 framework designed to create geospatial model-derived outdoor UAV datasets, combining ROS, Gazebo, and QGroundControl to simulate UAV missions and produce elevation-aware localization data.

Off-road robotic navigation has increasingly advanced through methods that integrate perception, learning, and planning to handle the challenges of unstructured terrain. Ref. [22] proposes a hierarchical multi robot framework (STALC) that leverages visibility-based environmental segmentation, topological graph planning through mixed-integer programming, and MPPI-driven local control for coordinated maneuvering in both simulation and field experiments. Ref. [23] propose RAMP, a risk-aware mapping and planning pipeline that improves 2.5D map reliability through ground-point inflation using an horizon MPPI planner to maximize speed and safety in complex 3D terrain, for hill-climbing scenarios.

Regarding learning based methods, ref. [24] present RoadRunner, a low-latency architecture that predicts traversability and elevation directly from fused camera LiDAR inputs, trained through self-supervised hindsight aggregation and validated in real-world off-road scenarios. Ref. [25] developed a multi-layer cost map that combines radiation levels, slope, and terrain traversability for A*-based navigation in hazardous environments, validated in simulation and physical tests. Lee et al. propose an uncertainty-aware navigation approach that learns terrain-induced disturbances from driving data, integrating uncertainties into traversability costs for planning in 3D terrain. Ref. [26] highlights persistent challenges in perception, scene understanding, and path planning in unstructured outdoor environments, emphasizing the importance of multimodal sensing and robust traversability reasoning for fully autonomous off-road operation.

Despite these advancements, a significant gap persists in autonomous, scalable techniques that convert publicly accessible geospatial data into ROS2-compatible, robot-specific, slope-aware traversability maps appropriate for multi-robot operations. Current methods generally depend on sensors mounted on robots, manual data preprocessing, or a restricted geographic range, limiting operational adaptability.

This study proposes an adaptive DEM-based mapping system that connects geospatial analysis with smart robotic perception, facilitating complete slope-aware costmap creation, real-time planning capabilities, and scalable multi-robot autonomy in intricate outdoor settings.

3. Methodology

The proposed line of work represents an intelligent perception layer for fleets of mobile robots in outdoor environments. The algorithm cv_gdal autonomously interprets the slope of the terrain, infers traversable regions, and generates maps. This autonomous perception reduces the reliance on an operator to manage search and rescue missions for mobile robotic fleets.

3.1. Problem Statement

The traversability maps generation strategy is based on the project's general requirements, so they must consider the restrictions imposed by the availability of physical robots. Examples of wheeled outdoor UGVs capable of using adaptive slope traversability maps are shown in Table 1.

Table 1. Commercial UGVs and their admisible slope.

Mobile Platform	Brand	Maximum Admissible Slope
Husky A200	Clearpath	45° (climb)/30° (traversal)
Husky A300	Clearpath	30°
Jackal	Clearpath	20°
Summit XL	Robotnik	38.6°
Panther	Husarion	44° (50 kg payload), 28° (100 kg payload)
Rover S7	SMP Robotics	30°
Rover S5	SMP Robotics	18°

The mobile robotic platform used for the simulation is the Clearpath Husky A200 (Figure 2), whose physical dimensions are 990 $\times$ 670 $\times$ 390 mm, four wheels with skid steering, 50 kg weight, maximum speed of 1 m/s, estimated autonomy of 4 h, and maximum incline of 30°.

Figure 2. Clearpath Robotics Husky A200.

The autonomy of each mobile robot is estimated to be 4 h, with a maximum speed of 1 m/s, so the routes should not exceed 12 km, considering round-trip distances.

Generated maps must be binarized in Portable Gray Map (PGM) format, according to ROS map conventions for restricted and movable space.

3.2. Materials

The simulation is performed on a 7th generation Intel Core i7 computer with a Nvidia GTX1070 graphics card, endowed with 16 GB of RAM. The system has been implemented for ROS2 Humble, with the tools described in Table 2.

Table 2. Tool description for system development.

O.S and ROS Framework	Description	Tool
ROS2 Humble (Ubuntu 22.04)	Simulator	Gazebo Classic
	Path planning tool	Nav2 (Navfn Global Planner)
	Navigation tool	Nav2 (DWB Local Planner)
	Robots model	Clearpath Robotics Husky

Satellite images are processed with OpenCV. For the generation of 3D models, the QGis tools (QGIS2threejs plugin) and Blender [27] are used for the export of textured meshes. Satellite images for the generation of DEM and navigation maps are obtained from the National Geographic Institute (IGN) of Spain, using raster images with digital elevation information of the areas of La Cabrera (Madrid), Rio Tinto Mines (Huelva), and Tenerife (Canary Islands).

3.3. Image Processing and Traversability Map Generation

The main contribution of this paper is the algorithm cv_gdal, which processes the satellite Geo TIFF (Tag Image File Format) image, detects changes in the gradient associated with elevation information, and generates an occupancy grid map depending on the slope overcoming capacity of a robot. In addition, a textured 3D model is created with the satellite image information for navigation and trajectory tracking tests in the Gazebo Classic simulation environment. It is divided into two stages:

- Three-dimensional mesh generation for Gazebo
- Generation of traversability maps

The tasks for 3D mesh and traversability maps generation are performed in parallel. QGIS and Blender are used to extract altitude and texture information from a GeoTIFF Image, while the cv_gdal algorithm is responsible for generating the grid occupancy map and its configuration file, whose parameters are necessary to generate the simulation.

Figure 3 presents the methodology used for this work, a multistage processing pipeline that transforms raw GeoTIFF data into accurate traversability map representations for realistic robot maneuvering. First, QGIS is used to enhance the DEM with satellite textures and to generate a textured 3D mesh through the QGIS2threejs plugin. In parallel, terrain gradients are computed using a Sobel-based operator, enabling slope estimation and an initial assessment of terrain traversability. These gradient maps are binarized according to the mobility constraints of the robot, yielding elevation-aware traversable regions. The resulting terrain layers are then exported as ROS-compatible map and configuration files, which serve as input for global and local costmap generation through the Nav2 navigation stack. By combining elevation gradients, DEM geometry, textural information, and robot-specific constraints, this digital map processing workflow ensures that the generated maps reflect realistic terrain structure and the operational limitations of the UGVs, enabling realistic maneuvering and multi-robot navigation in simulation.

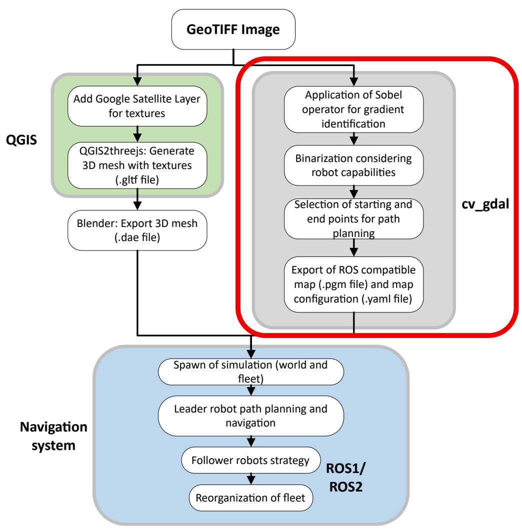

Figure 3. Description of the system workflow and cv_gdal phases. Source: Authors.

3.3.1. Three-Dimensional Mesh Generation for Gazebo

The first step is to identify the area of interest (post-disaster zone or geographical accident) to explore and evaluate the availability and accessibility of GeoTIFF files. In this context, there are reliable public datasets or government sources, such as the National Aeronautics and Space Administration (NASA), the European Space Agency (ESA), and the Copernicus Open Access Hub [21].

For this work, the source is the Spanish National Geographic Institute (IGN), an organization that has geospatial data under the Cloud Optimized GeoTIFF (COG) standard with a resolution of up to 2 m (in specific areas).

The TIFF images correspond to areas with extensions of several kilometers; in order to crop these images and extract geospatial information, OpenCV, GDAL, and rasterio libraries are used. The selected areas are detailed in Table 3.

Table 3. Geo spatial characteristics of selected maps.

Item	Zone	City	Geodesic System	Lat/Lon Start	Lat/Lon End	Dimension of Map (Meters)
1	La Cabrera	Madrid	WGS84	40.8767448, −3.6052464	40.86395, −3.5881617	(1430.0, 1430.0)
2	Pico Miel	Madrid	WGS84	40.88779429, −3.62455311	40.8760248, −3.59472480	(2504.0, 1324.0)
3	Rio Tinto Mines	Huelva	WGS84	37.7092916, −6.5925750	37.6947515, −6.57519564	(1574.0, 1574.0)
4	Rio Tinto Mines	Huelva	WGS84	37.7102749, −6.61522892	37.697782, −6.59029368	(2234.0, 1330.0)
5	Timanfaya National Park	Canary Islands	WGS84	28.9936552, −13.81737497	28.9790830, −13.7724011	(4398.0, 1570.0)
6	Tenerife	Canary Islands	WGS84	28.2700312, −16.8429782	28.257783, −16.8168416	(2543.7, 1396.0)

The 3D model generation workflow shown in Figure 4 summarizes the pipeline used to obtain a textured terrain representation ready for simulation from geospatial data sources. Initially, for the application of the texture layer, QGIS [28] is used, importing the acquired TIFF image and adding the Google Satellite Imagery layer to export the scene in glTF format (Graphics Library Transmission Format) through the QGIS2threejs plugin.

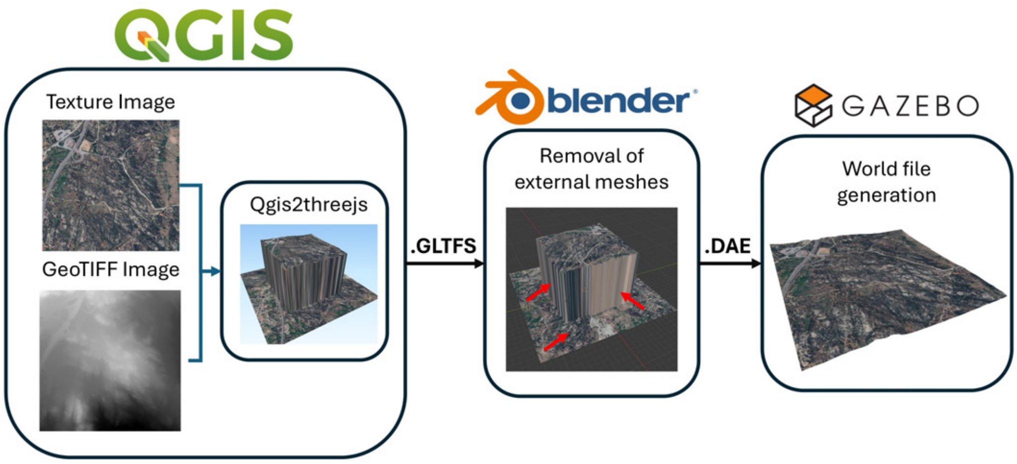

Figure 4. Three-dimensional model generation of terrain using QGIS and Blender. Source: Authors.

The abrupt height discontinuities in the GLTF model arise from the lack of elevation information in the RGB orthophoto. To avoid inconsistencies in the cropping operations performed in QGIS, a larger scene is exported, which introduces an artificial flat base that does not correspond to the actual topography of the target area. To maintain topological consistency within the reconstructed surface, the lower plane is manually removed in

https://doi.org/10.3390/app16073351

Blender, retaining only the sections supported by valid elevation data. The georeferenced RGB orthophoto, aligned with the original GeoTIFF, was then re-projected onto the cleaned mesh to preserve spatial detail while ensuring scalable resolution for subsequent navigability analysis. Finally, the processed model was exported in DAE (Collada) format, enabling the generation of 3D models and simulation environments compatible with Gazebo Classic.

Although Gazebo is natively compatible with TIFF files for Simulation Description Format (SDF) generation, since the file is a large-scale model, the calculation of physics when in contact with the wheels of the robots has a high computational cost, reducing the real-time factor of the simulation to 0.05. When working with a textured mesh, this factor increases to 0.9, significantly reducing simulation time.

3.3.2. Generation of Traversability Maps

For the application of DEMs used in robot navigation, it is necessary to integrate 2.5D information into a 2D plane, so OpenCV libraries are used for image processing, along with the Geospatial Data Abstraction Library (GDAL) [29] and rasterio [30], for the processing of geospatial images. To obtain the gradient maps, edge detection algorithms are applied, whose differential operators calculate the gradient approximation over the pixels of the raster image.

The Sobel operator applies the combination of an intensity gradient operator for each pixel of the image and a smoothing filter, making it less sensitive to noise, yelding the norm and direction of the vector for each pixel can be obtained as a result.

This operator is applied for the north and east directions and is then superimposed. The discrete function that defines the combination of the derivatives on both axes is represented by the discretized gradient vector shown in Equation (1).

$$\nabla f(x_i, y_i) = (f_{(i+1,j)} - f_{(i,j)}, f_{(i,j+1)} - f_{(i,j)}) \tag{1}$$

This operator can be different depending on the application; for edge detection, the operators in the North (x) and East (y) axes are the following:

$$K_x = \begin{bmatrix} -1 & 0 & 1 \\ -2 & 0 & 2 \\ -1 & 0 & 1 \end{bmatrix}, K_y = \begin{bmatrix} 1 & 2 & 1 \\ 0 & 0 & 0 \\ -1 & -2 & -1 \end{bmatrix} \tag{2}$$

Thus, the approximations of the intensity gradient for an image are calculated in Equation (3).

$$G_x = K_x * I, G_y = K_y * I \tag{3}$$

where I is the image, G_x the north axis approximation, and G_y the east axis approximation. To calculate the magnitude and direction of the gradient, Equation (4) is applied:

$$G = \sqrt{{G_x}^2 + {G_y}^2}, \theta = \arctan(G_y, G_x) \tag{4}$$

To obtain edges, different first derivative operators (Roberts, Prewitt) and second derivative operators (Laplacian, Laplacian of a LOG Gaussian), as well as the Canny operator, have been tested.

The Sobel operator has been selected because it offers the best results for the application on GeoTIFF images. Subsequently, the image is binarized with a threshold value defined by the maximum traversable slope of the mobile robot, allowing for the selection of the starting and end points. Additionally, the size of the original TIFF image is increased by a rescaling factor to improve the resolution of the global planner in the navigation stage.

The Algorithm 1 shows the pseudocode implemented for this phase, using the GeoTIFF image as the input variable. The following functions explain the processes:

- get_res: Obtains the resolution from the GeoTIFF file with rasterio.
- get_map_size: Obtains the map size in meters from the GeoTIFF file with rasterio.
- apply_sobel: Applies the Sobel operator to an image. Returns a slope image.
- get_threshold: Captures the admissible slope value from a GUI slider
- gui_selection: Gets the values of the coordinates of x, y for the starting (first click) and end (second click) points. Returns two tuples of pixel positions.
- binarize: OpenCV function to binarize the image with the selected threshold.
- resize_map: Resizes original TIFF file.
- save_config: Exports map configuration file in YAML format.

Algorithm 1 Traversability map generation

Input: $input\_tiff$
Output: $map_{image}, map_{config}$

//slider: slider in GUI $(modifiable)$
//zone_name: name of processed GeoTIFF
//resize_factor: resize scale for higher resolution $(between 1 - 10)$
$x_{init} = y_{init} = x_{end} = y_{end} = None$
$threshold = None$
$resolution \leftarrow get\_res(input\_tiff)$
$map\_size \leftarrow get\_map\_size(input\_tiff)$
$magnitude \leftarrow apply\_sobel(input\_tiff)$
while $(x_{init}$ OR y_{init} OR x_{end} OR $y_{end}) == None$ **do**
    $threshold = get\_threshold(slider)$
    $state\_click = check\_click(input_{tiff})$
    if $state\_click == 2$ **then**
        $x_{init}, y_{init}, x_{end}, y_{end} \leftarrow gui\_selection(input\_tiff)$
    end if
end while
$binary\_map \leftarrow binarize(magnitude, threshold)$
$map_{image} \leftarrow resize\_map(binary\_map, resize\_factor)$
$map_{config} \leftarrow save\_config(x_{init}, y_{init}, x_{end}, y_{end}, resolution, zone\_name, map\_size)$
return $map_{image}, map_{config}$

For navigation, two necessary files are generated: map image (.pgm) and map configuration (.yaml). The parameters used in the configuration file are:

- Image: Path to the image that map_server node loads
- Resolution: Resolution of the map in meters/pixel
- Origin: Start 2D pose of the leader robot in the lower-left pixel in map
- Destiny: End 2D of the leader robot in the lower-left pixel in map
- Map_size: Map size in meters
- Zone_name: Zone name of processed TIFF file
- Negate: Reversed interpretation of White (free)/black (occupied) semantics
- Occupied_thresh: Threshold for occupancy probability. Higher is occupied
- Free_thresh: Threshold for occupancy probability. Lower values correspond to free space.

The map image and map configuration are used for the generation of local and global cost maps for autonomous navigation of the robotic fleet. The process for generating the traversability map from the TIFF file is shown in Figure 5. This workflow corresponds to the steps described in Algorithm 1.

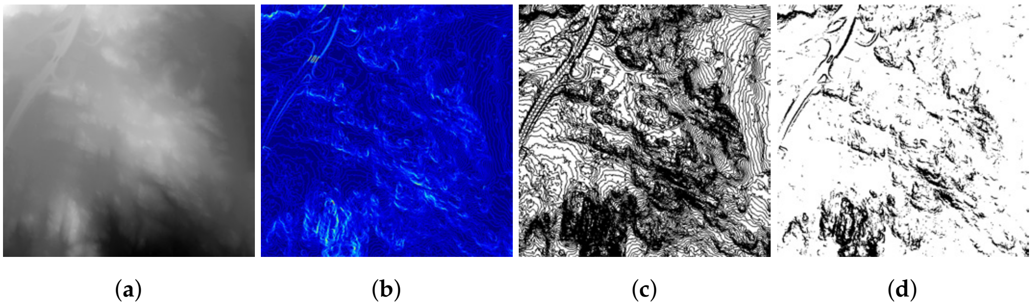

Figure 5. TIFF image processing to binary map for fleet navigation in zone La Cabrera. (**a**) original TIFF image, (**b**) slope map, (**c**) map with admissible slope 10%, (**d**) map with admissible slope of 30%. Source: Authors.

3.4. Multirobot Navigation Using Shared Terrain Information

The proposed approach adopts an online leader–follower strategy that enables coordinated multi-robot movement over off-road terrain. Once the traversability map is generated, the leader robot evaluates the elevation-aware map and computes a traversable global path that takes into account slope variations, static and dynamic obstacles. This feasible leader-generated path incorporates terrain constraints that would be challenging for individual robots to estimate independently.

To enable collective navigation, the traversability map and the leader's planned route are shared with all follower robots through Nav2. Each follower receives a feasible goal that has already been achieved by the leader robot, performing path planning according to its own footprint, mobility constraints, and local sensing feedback. This online reinterpretation allows robots of different sizes or capabilities to track variants of the leader's path while ensuring traversability and maneuverability. The shared map provides a common understanding of the environment, while the individualized refinement ensures that narrow passages, steep transitions, or high-risk locations are handled differently by each robot, depending on its specific characteristics. By combining shared environmental information with the leader–follower online strategy, the fleet maintains cohesive movement while ensuring that each agent navigates along a version of the route physically feasible for its platform. This methodology improves collective mobility, reduces redundant terrain evaluation, and supports robust multi-robot maneuvering in unstructured off road environments.

4. Results

This chapter presents the results obtained. For the DEM generation section, the 3D models of the selected zones are shown in Figure 6.

In order to create a world file accepted by Gazebo, lighting, gravity, and friction characteristics are added to the scene; these parameters are described in the XML file using the Open Dynamics Engine (ODE) plugin and applied to the collision mesh of the model.

The simulation environments resulting from the DEMs processed after the textured meshes are deployed in Gazebo are shown in Figure 7, demonstrating the integration of the terrain models with the configured physics settings.

The different slope maps obtained from the TIFF files are represented in Figures 8–13.

After applying the binarization step based on admissible slope, the corresponding traversability maps are generated. These maps encode the regions classified as navigable or non-navigable according to the mobility constraints defined for the robotic platform. A visual representation of the generated traversability maps is shown in Figures 14–19.

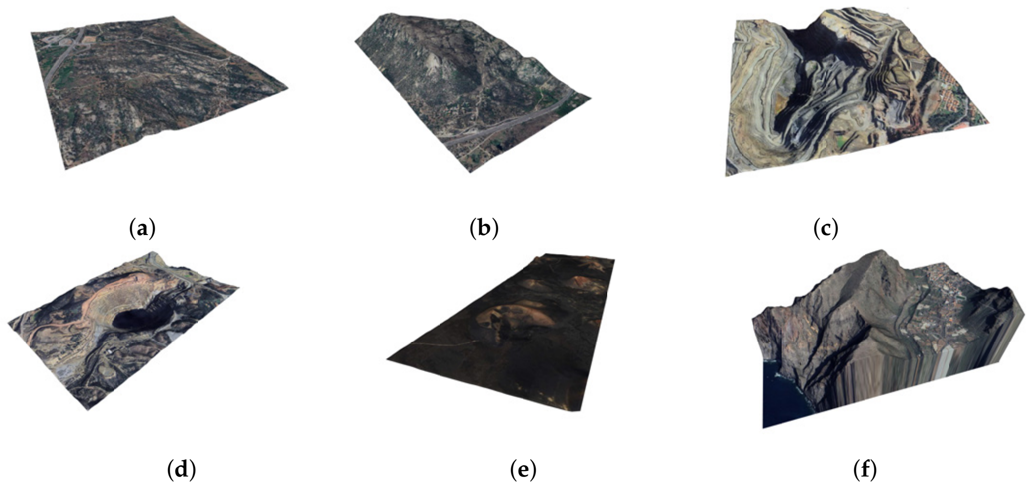

Figure 6. Generated 3D models of selected zones with applied textures. (**a**) La cabrera, (**b**) Pico Miel, (**c**) Rio Tinto Mines 1, (**d**) Rio Tinto Mines 2, (**e**) Timanfaya, (**f**) Tenerife. Source: Authors.

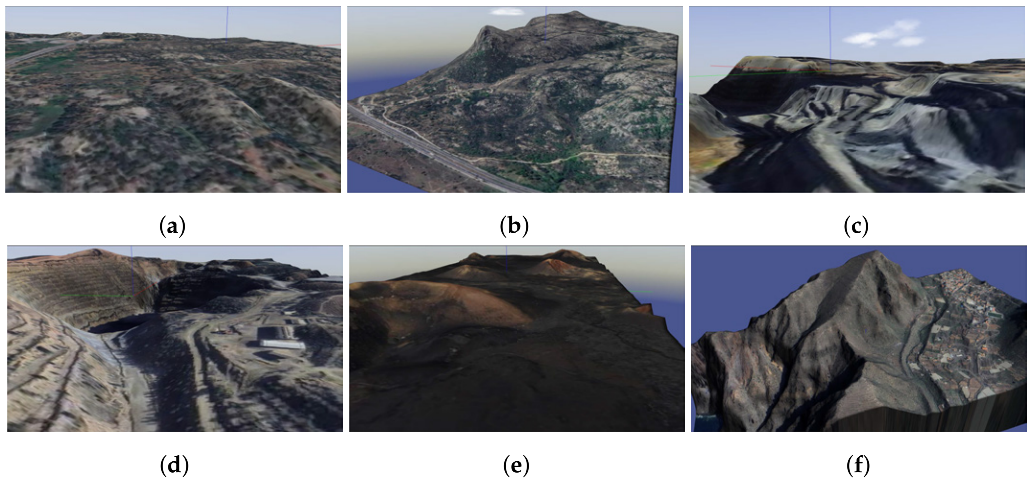

Figure 7. Digital elevation models in Gazebo. (**a**) La cabrera, (**b**) Pico Miel, (**c**) Rio Tinto Mines 1, (**d**) Rio Tinto Mines 2, (**e**) Timanfaya, (**f**) Tenerife. Source: Authors.

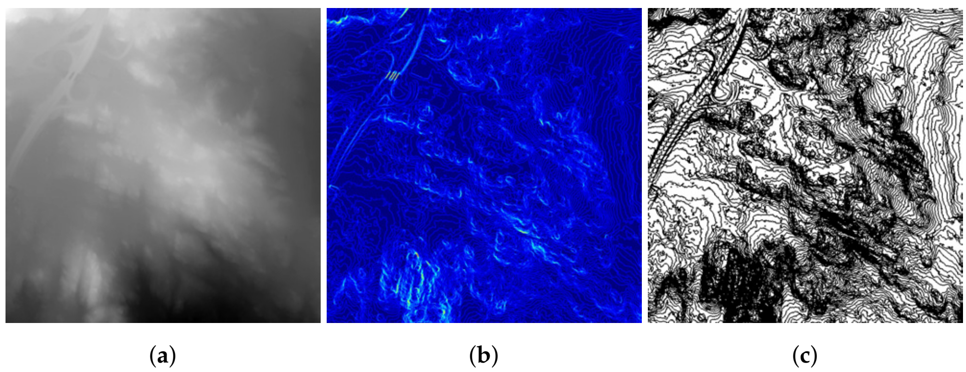

Figure 8. Visual representation of (**a**) original TIFF files, (**b**) slope map, (**c**) binary map for 0% admisible slope for La Cabrera map. Source: Authors.

https://doi.org/10.3390/app16073351

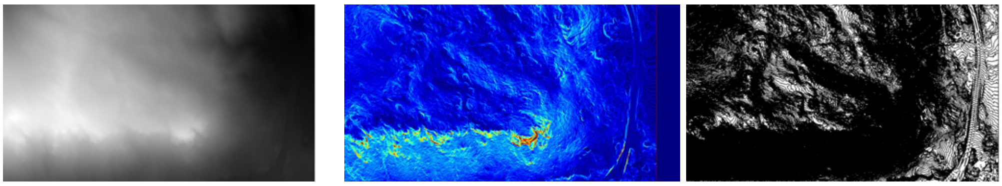

(a) (b) (c)

Figure 9. Visual representation of (**a**) original TIFF files, (**b**) slope map, (**c**) binary map for 0% admisible slope for Pico Miel map. Source: Authors.

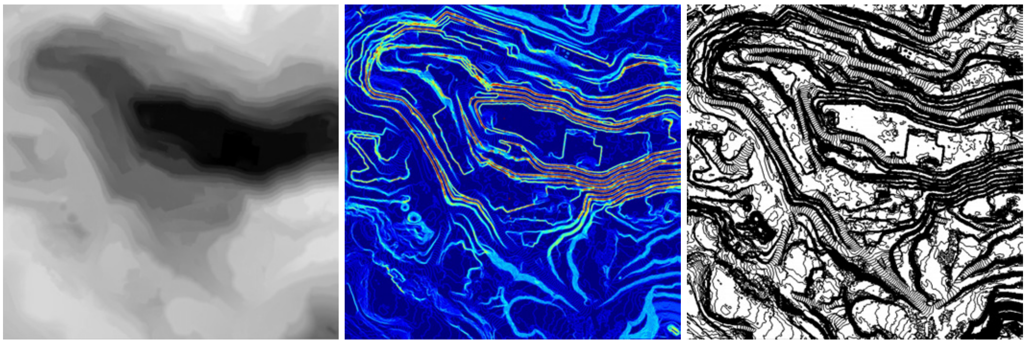

(a) (b) (c)

Figure 10. Visual representation of (**a**) original TIFF files, (**b**) slope map, (**c**) binary map for 0% admisible slope for Rio Tinto Mines 1 map. Source: Authors.

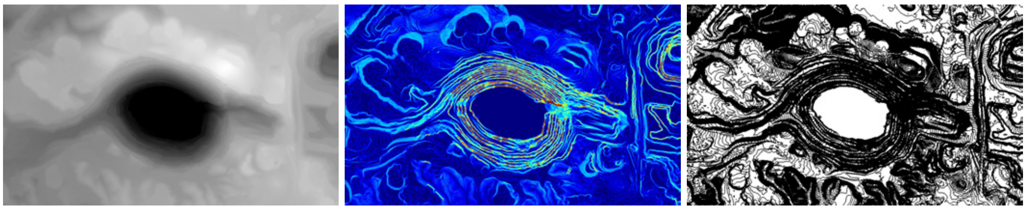

(a) (b) (c)

Figure 11. Visual representation of (**a**) original TIFF files, (**b**) slope map, (**c**) binary map for 0% admisible slope for Rio Tinto Mines 2 map. Source: Authors.

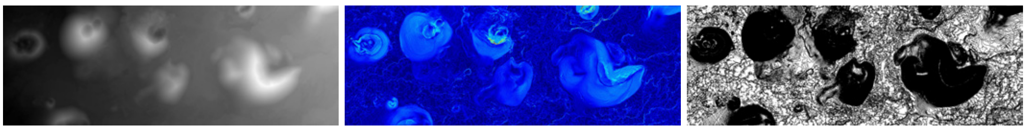

(a) (b) (c)

Figure 12. Visual representation of (**a**) original TIFF files, (**b**) slope map, (**c**) binary map for 0% admisible slope for Timanfaya map. Source: Authors.

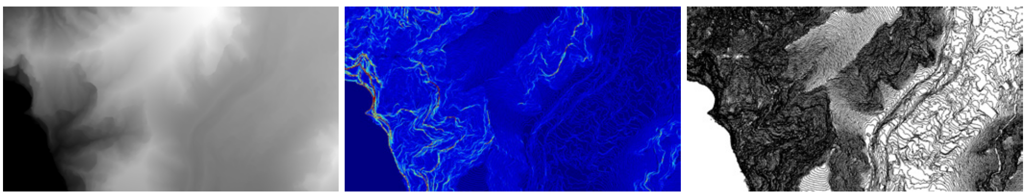

(a) (b) (c)

Figure 13. Visual representation of (**a**) original TIFF files, (**b**) slope map, (**c**) binary map for 0% admisible slope for Canarias map. Source: Authors.

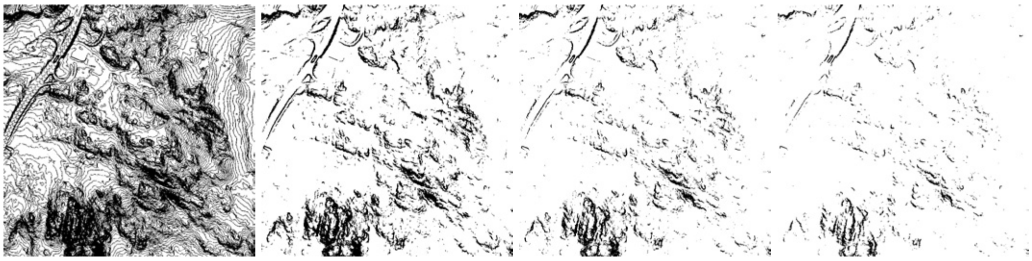

(**a**) (**b**) (**c**) (**d**)

Figure 14. Traversability maps for navigation at different slopes, (**a**) 20%, (**b**) 30%, (**c**) 40%, (**d**) 50% for La Cabrera map. Source: Authors.

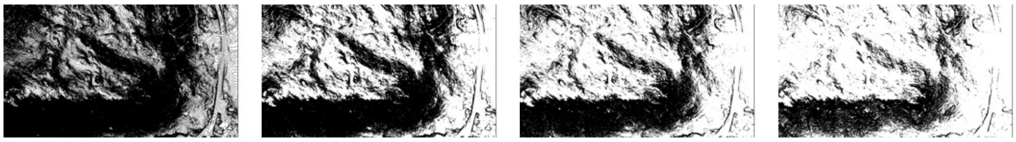

(**a**) (**b**) (**c**) (**d**)

Figure 15. Traversability maps for navigation at different slopes, (**a**) 20%, (**b**) 30%, (**c**) 40%, (**d**) 50% for Pico Miel map. Source: Authors.

(**a**) (**b**) (**c**) (**d**)

Figure 16. Traversability maps for navigation at different slopes, (**a**) 20%, (**b**) 30%, (**c**) 40%, (**d**) 50% for Rio Tinto Mines 1 map. Source: Authors.

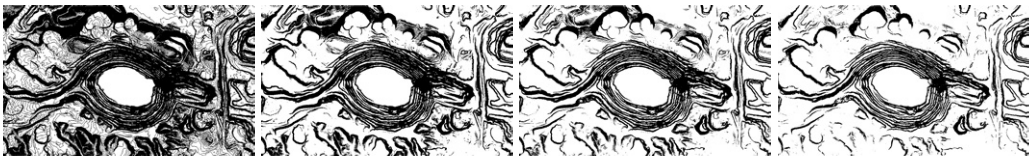

(**a**) (**b**) (**c**) (**d**)

Figure 17. Traversability maps for navigation at different slopes, (**a**) 20%, (**b**) 30%, (**c**) 40%, (**d**) 50% for Rio Tinto Mines 2 map. Source: Authors.

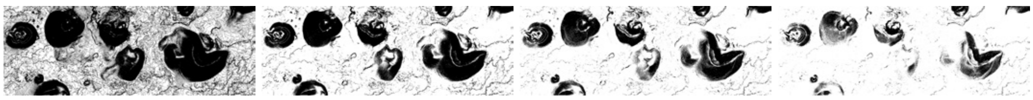

(**a**) (**b**) (**c**) (**d**)

Figure 18. Traversability maps for navigation at different slopes, (**a**) 20%, (**b**) 30%, (**c**) 40%, (**d**) 50% for Timanfaya map. Source: Authors.

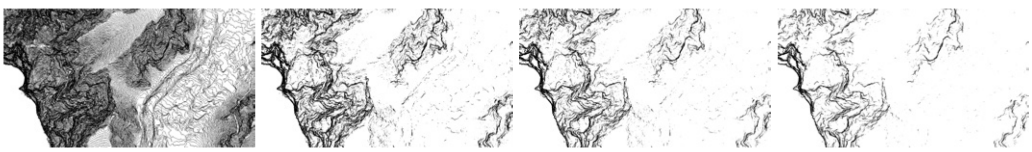

(**a**) (**b**) (**c**) (**d**)

Figure 19. Traversability maps for navigation at different slopes, (**a**) 20%, (**b**) 30%, (**c**) 40%, (**d**) 50% for Canarias map. Source: Authors.

Application of traversability maps to multirobot navigation tasks is shown in Figure 20.

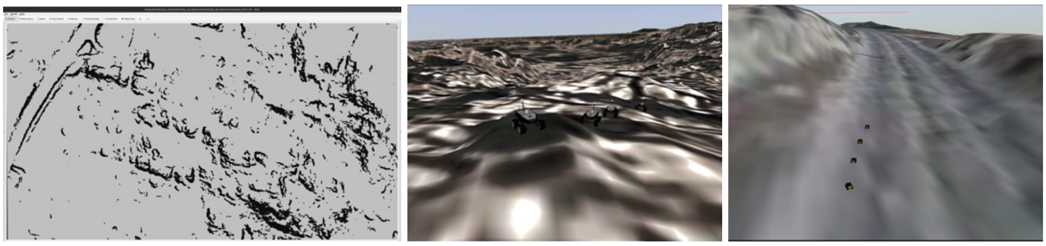

(**a**) (**b**) (**c**)

Figure 20. System navigation for multirobot fleet test in ROS Framework. (**a**) Generated traversability map in RViz, (**b**) simulation in Gazebo Classic, (**c**) simulation in Gazebo Classic. Source: Authors.

Finally, the traversability map integration and experiments for the multirobot system navigation tests are shown in Figures 21–24.

Navigation integrates positive obstacle avoidance and awareness of other fleet robots, as well as the local costmap evasion of morphological anomalies arising from 3D world model generation inconsistencies.

A total of 60 navigation experiments were conducted with 10 trials per zone. Each region included two distance regimes: five short-range experiments with goal distances between 80 m and 200 m, and five long-range experiments with distances between 1.0 km and 1.4 km, with a maximum linear speed of 0.5 m/s and an angular speed of 1 rad/s constraints for each robot.

All digital terrain models were processed at a spatial resolution of 0.1 m per pixel, ensuring high-fidelity elevation and slope extraction. The proposed mapping pipeline, responsible for generating slope maps, binary traversability layers, and ROS-compatible maps, operated with 100% stability, producing correct outputs with an average processing time of less than 2 s, being competitive for large-scale environments, demonstrating the feasibility of on-demand automated global map generation, addressing a common limitation in DEM-based navigation approaches.

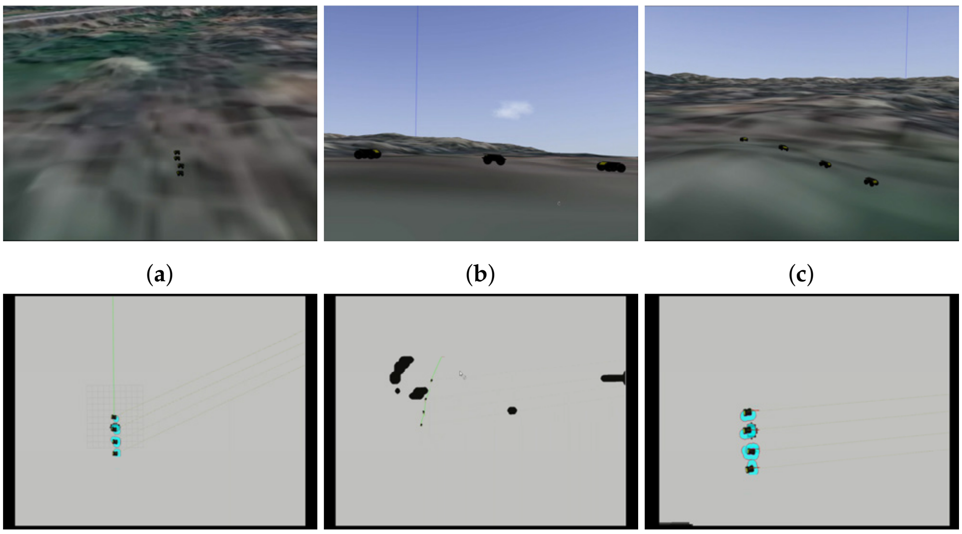

(**a**) (**b**) (**c**)

(**d**) (**e**) (**f**)

Figure 21. System navigation test through La Cabrera map. (**a**,**d**) Initial configuration, (**b**,**e**) multirobot node-edge configuration, (**c**,**f**) arrival configuration. Source: Authors.

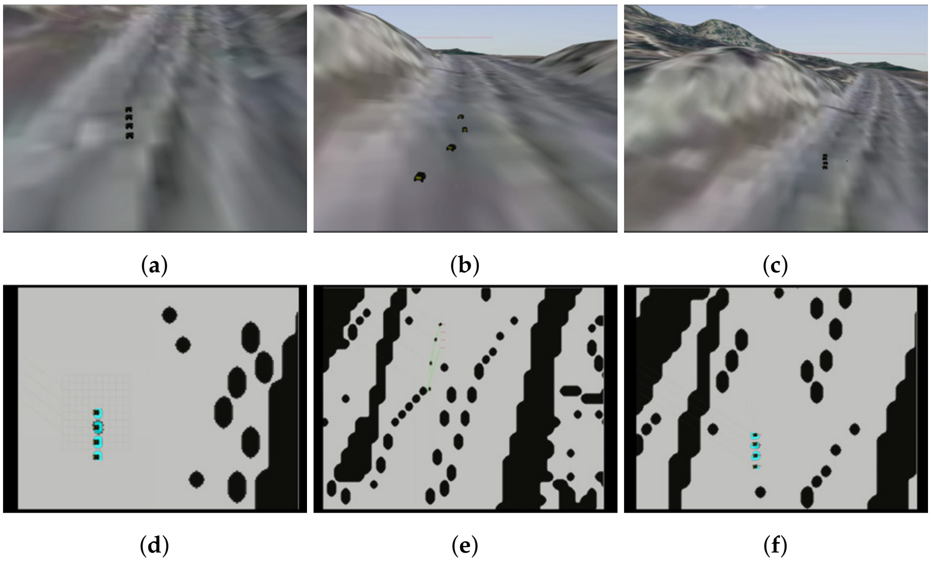

Figure 22. System navigation test through Pico Miel map. (a,d) Initial configuration, (b,e) multirobot node-edge configuration, (c,f) arrival configuration. Source: Authors.

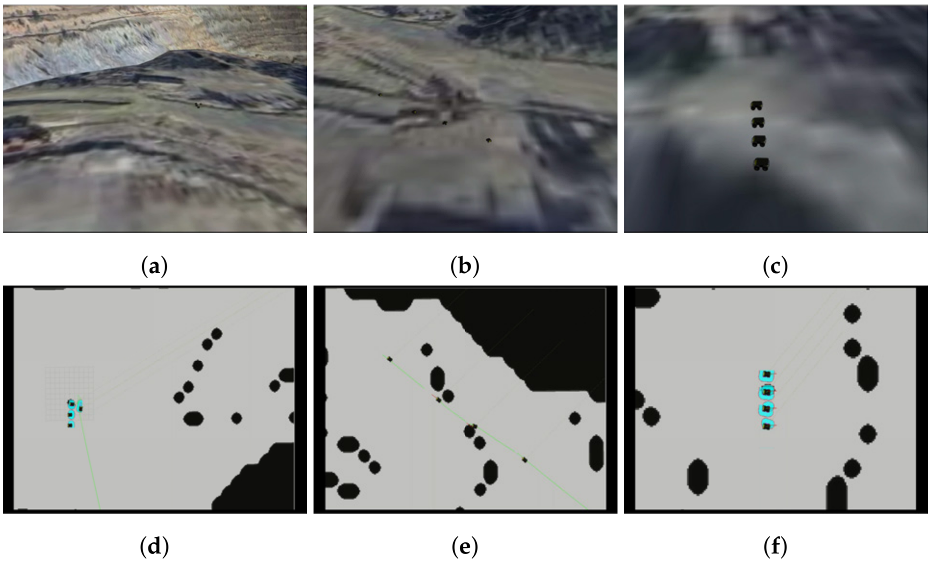

Figure 23. System navigation test through Rio Tinto Mines 2 map. (a,d) Initial configuration, (b,e) multirobot node-edge configuration, (c,f) arrival configuration. Source: Authors.

Due to Gazebo's limited support for high-resolution GeoTIFF terrain, the simulation environment required manual conversion to DAE (Collada); however, this step introduced no errors in world construction or map integration. Reliance on simulation introduces inherent limitations on the dynamic representation of the environment, like micro-roughness, soil-wheel interaction, or sensor noise, which cannot be fully reproduced, meaning that real-world performance can differ, particularly in terrains with deformable or high variable surfaces.

Regarding navigation performance, the system successfully executed 52 of 60 tests, leading to an overall success rate of 86.7%, while 8 tests (13.3%) resulted in failures caused by the navigation subsystem. Most failures occurred in regions with abrupt elevation gradients in which the inflation parameters of the local planner and the interpretation of the obstacles caused conservative path blocking. This indicates that while the global DEM-based costmap provides strong guidance, certain local behaviors, especially near steep slopes or narrow traversable corridors, require further tuning. Additionally, fleet-level interactions were effectively handled, with no deadlocks or blocking events observed, although minor delays were detected when the leader robot replanted the path.

In general, the results indicate that the proposed DEM-based traversability framework performs reliably under diverse terrain conditions. The system demonstrated robust performance, fast processing times, and adaptive behavior in all regions evaluated.

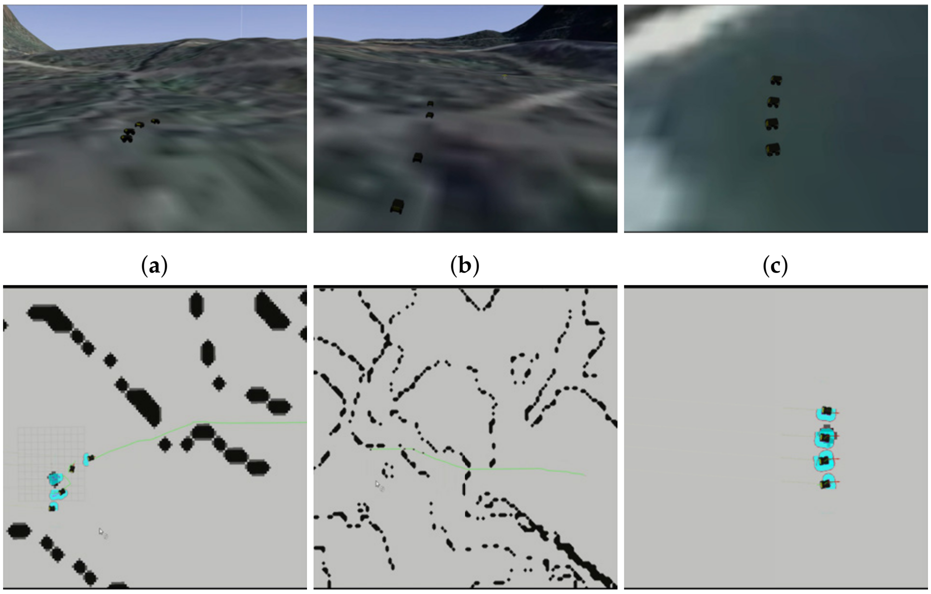

(a) (b) (c) (d) (e) (f)

Figure 24. System navigation test through Canarias map. (**a**,**d**) Initial configuration, (**b**,**e**) multirobot node-edge configuration, (**c**,**f**) arrival configuration. Source: Authors.

5. Conclusions

This paper presents a novel methodology for processing GeoTIFF satellite imagery and generating traversability maps based on the slopes that a mobile robot can overcome according to its physical characteristics.

The generated DEMs feature different degrees of traversability and serve as a simulation framework to test various fleet coordination and reconfiguration algorithms, as well as navigation strategies that consider different terrain and dynamic constraints.

Applying a proper rescaling factor to the traversability map is essential for navigation, as it affects both the size of the PGM image and the resolution specified in the map's YAML file. However, the configuration of parameters in Nav2 presents problems with high resolution values, while extensive maps cause failures at the ROS *map_server* node.

The terrain processing pipeline demonstrated consistent performance across evaluated scenarios, confirming its robustness. The generation of high-resolution traversability layers and their integration into the ROS framework proceeded without incident, highlighting the stability of the mapping approach. By contrast, the limitations observed during navigation were attributable to the behavior of the simulated planning and control modules rather than to deficiencies in the terrain processing method.

Future work should focus on optimizing the strategies applied in this study, such as smoothing planned paths, optimizing algorithms for integration into onboard computers, and executing the proposed algorithm for real deployment missions.

Author Contributions: Conceptualization, D.O., J.M.B. and J.d.C.; methodology, A.B., D.O. and C.C.U.; software, J.M.B., D.O.; validation, D.O., C.C.U. and J.M.B.; formal analysis, D.O., J.d.C. and A.B.; investigation, J.M.B., D.O., C.C.U., A.B. and J.d.C.; resources, A.B. and J.d.C.; data curation, D.O., J.M.B. and C.C.U.; writing—original draft preparation, D.O., C.C.U. and J.d.C.; writing—review and editing, D.O., C.C.U. and A.B.; visualization, C.C.U., A.B. and J.d.C.; supervision, J.d.C., and

A.B.; project administration, A.B. and J.d.C.; funding acquisition, A.B. and J.d.C. All authors have read and agreed to the published version of the manuscript.

Funding: This research was funded by Project "CollaborativE Search And Rescue robots (CESAR)" (PID2022-142129OB-I00) founded by MCIN/AEI/10.13039/501100011033, by FEDER/EU and Dirección General de Investigación e Innovación Tecnológica, Vicepresidencia, Consejería de Educación y Universidades de la Comunidad de Madrid (ORDER 3789/2022 Ayudas para la Contratación de Personal Investigador Predoctoral (PIPF-2022/TEC-25073).

Institutional Review Board Statement: Not applicable.

Informed Consent Statement: Not applicable.

Data Availability Statement: A video description of the article can be found in Appendix A. The reported data and the algorithm cv_gdal can be found in Appendix B. The package for multirobot simulation in gazebo can be found in Appendix C.

Acknowledgments: Special thanks to the Robotics and Cybernetics Group of the Center for Automatics and Robotics for the help with resources to carry out this research.

Conflicts of Interest: The authors declare no conflict of interest.

Abbreviations

The following abbreviations are used in this manuscript:

ROS	Robot Operating System
SAR	Search and Rescue
UGV	Unmanned Ground Vehicle
DEM	Digital Elevation Model
TIFF	Tagged Image File Format
RRT	Rapid Random Trees
WiSAR	Wilderness SAR

Appendix A

Link to the video: (accessed on 26 February 2025). https://youtu.be/YBqy-xaQaf4.

Appendix B

Algorithm cv_gdal and results can be found on https://github.com/davicktm92/cv_gdal (accessed on 26 February 2025).

Appendix C

The developed package for multi-robot simulation, including namespaced Nav2 nodes, can be found in https://github.com/davicktm92/husky_multirobot (accessed on 26 February 2025).

References

1. Orbea, D.; Ulloa, C.C.; Del Cerro, J.; Barrientos, A. Mobile CDPR System for Robotic Sinkhole Exploration. In *2024 10th International Conference on Automation, Robotics, and Applications, ICARA 2024*; Institute of Electrical and Electronics Engineers Inc.: New York, NY, USA, 2024; pp. 347–351. [CrossRef]
2. Howard, A.; Seraji, H. An intelligent terrain-based navigation system for planetary rovers. *IEEE Robot. Autom. Mag.* **2001**, *8*, 9–17. [CrossRef]
3. Papadakis, P. Terrain traversability analysis methods for unmanned ground vehicles: A survey. *Eng. Appl. Artif. Intell.* **2013**, *26*, 1373–1385. [CrossRef]
4. Grohmann, C.H.; Smith, M.J.; Riccomini, C. Multiscale analysis of topographic surface roughness in the Midland Valley, Scotland. *IEEE Trans. Geosci. Remote Sens.* **2011**, *49*, 1200–1213. [CrossRef]

5. Sánchez, M.; Morales, J.; Martínez, J.L. Waypoint Generation in Satellite Images Based on a CNN for Outdoor UGV Navigation. *Machines* **2023**, *11*, 807. [CrossRef]
6. Atas, F.; Cielniak, G.; Grimstad, L. From Simulation to Field: Learning Terrain Traversability for Real-World Deployment. *arXiv* **2025**. [CrossRef]
7. Haddeler, G.; Chuah, M.Y.; You, Y.; Chan, J.; Adiwahono, A.H.; Yau, W.Y.; Chew, C.M. Traversability analysis with vision and terrain probing for safe legged robot navigation. *Front. Robot. AI* **2022**, *9*, 887910. [CrossRef]
8. Julius Fusic, S.; Kanagaraj, G.; Hariharan, K.; Karthikeyan, S. Optimal path planning of autonomous navigation in outdoor environment via heuristic technique. *Transp. Res. Interdiscip. Perspect.* **2021**, *12*, 100473. [CrossRef]
9. Prinz, R.; Bulbul, R.; Scholz, J.; Eder, M.; Steinbauer-Wagner, G. Off-Road Navigation Maps for Robotic Platforms using Convolutional Neural Networks. *AGILE Giscience Ser.* **2022**, *3*, 55. [CrossRef]
10. Manderson, T.; Manjanna, S.; Dudek, G. Heterogeneous Robot Teams for Informative Sampling. *arXiv* **2019**. [CrossRef]
11. Bernal, A.; Muñoz, C.; Sáez, A.; Serrano-López, R. Suitability of the Spanish Open Public Cartographic Resources for BIM Site Modeling. *PFG-J. Photogramm. Remote Sens. Geoinf. Sci.* **2021**, *89*, 505–517. [CrossRef]
12. Wang, L.; Ai, T.; Shen, Y.; Li, J. The isotropic organization of DEM structure and extraction of valley lines using hexagonal grid. *Trans. GIS* **2020**, *24*, 483–507. [CrossRef]
13. Niemeyer, J.; Rottensteiner, F.; Soergel, U. Contextual classification of lidar data and building object detection in urban areas. *ISPRS J. Photogramm. Remote Sens.* **2014**, *87*, 152–165. [CrossRef]
14. Galar, M.; Sesma, R.; Ayala, C.; Albizua, L.; Aranda, C. Super-resolution of Sentinel-2 images using convolutional neural networks and real ground truth data. *Remote Sens.* **2020**, *12*, 2941. [CrossRef]
15. Wellhausen, L.; Dosovitskiy, A.; Ranftl, R.; Walas, K.; Cadena, C.; Hutter, M. Where should i walk(Predicting terrain properties from images via self-supervised learning. *IEEE Robot. Autom. Lett.* **2019**, *4*, 1509–1516. [CrossRef]
16. Meng, X.; Hatch, N.; Lambert, A.; Li, A.; Wagener, N.; Schmittle, M.; Lee, J.; Yuan, W.; Chen, Z.; Deng, S.; et al. TerrainNet: Visual Modeling of Complex Terrain for High-speed, Off-road Navigation. *arXiv* **2023**, arXiv:2303.15771.
17. Fortuna, S.; Chiodini, S.; Valmorbida, A.; Pertile, M. ROS 2 Integrated Continuous Terrain Mapping Comparison for Autonomous Navigation in Unstructured Environments. In *2024 IEEE International Workshop on Metrology for AeroSpace, MetroAeroSpace 2024-Proceeding*; Institute of Electrical and Electronics Engineers Inc.: New York, NY, USA, 2024; pp. 128–133. [CrossRef]
18. Liu, J.; Chen, X.; Xiao, J.; Lin, S.; Zheng, Z.; Lu, H. Hybrid Map-Based Path Planning for Robot Navigation in Unstructured Environments. In *IEEE International Conference on Intelligent Robots and Systems*; Institute of Electrical and Electronics Engineers Inc.: New York, NY, USA, 2023; pp. 2216–2223. [CrossRef]
19. Jeon, Y.; Son, E.I.; Seo, S.W. Follow the Footprints: Self-supervised Traversability Estimation for Off-road Vehicle Navigation based on Geometric and Visual Cues. In *Proceedings-IEEE International Conference on Robotics and Automation*; Institute of Electrical and Electronics Engineers Inc.: New York, NY, USA, 2024; pp. 1774–1780. [CrossRef]
20. Chong, Z.; Quin, B.; Bandyopadhyay, T.; Ang, M., Jr.; Frazzoli, E.; Rus, D. *2013 IEEE/RSJ International Conference on Intelligent Robots and Systems (IROS)*; IEEE: New York, NY, USA, 2013.
21. Jarraya, I.; Abdelkader, M.; Gabr, K.; Kadri, M.B.; Alahmed, F.; Boulila, W.; Koubaa, A. OS-RFODG: Open-Source ROS2 Framework for Outdoor UAV Dataset Generation. *Results Eng.* **2025**, *27*, 106613. [CrossRef]
22. Dimmig, C.A.; Goertz, A.; Polevoy, A.; Gonzales, M.; Yeh, B.; Wolfe, K.C.; Woosley, B.; Rogers, J.; Moore, J. Multi-Robot Planning for Coordinated Off-road Maneuvers. In Proceedings of the ICRA2024 Workshop on Resilient Off-road Autonomy, Yokohama, Japan, 17 May 2024.
23. Sharma, L.; Everett, M.; Lee, D.; Cai, X.; Osteen, P.; How, J.P. RAMP: A Risk-Aware Mapping and Planning Pipeline for Fast Off-Road Ground Robot Navigation. In Proceedings of the 2023 IEEE International Conference on Robotics and Automation (ICRA), London, UK, 29 May–2 June 2023.
24. Frey, J.; Patel, M.; Atha, D.; Nubert, J.; Fan, D.; Agha, A.; Padgett, C.; Spieler, P.; Hutter, M.; Khattak, S. RoadRunner—Learning Traversability Estimation for Autonomous Off-Road Driving. *IEEE Trans. Field Robot.* **2024**, *1*, 192–212. [CrossRef]
25. Huang, Y.; Shi, X.; Zhou, Y.; Xiong, Z. Autonomous navigation of mobile robot in radiation environment with uneven terrain. *Int. J. Intell. Robot. Appl.* **2023**, *7*, 497–509. [CrossRef]
26. Wijayathunga, L.; Rassau, A.; Chai, D. Challenges and Solutions for Autonomous Ground Robot Scene Understanding and Navigation in Unstructured Outdoor Environments: A Review. *Appl. Sci.* **2023**, *13*, 9877. [CrossRef]
27. Blender Foundation. Available online: https://www.blender.org/ (accessed on 26 February 2025).
28. Rosas-Chavoya, M.; Gallardo-Salazar, J.L.; López-Serrano, P.M.; Alcántara-Concepción, P.C.; León-Miranda, A.K. Qgis a constantly growing free and open-source geospatial software contributing to scientific development. *Geogr. Res. Lett.* **2022**, *48*, 197–213. [CrossRef]

https://doi.org/10.3390/app16073351

29. Lemenkova, P.; Debeir, O. GDAL and PROJ Libraries Integrated with GRASS GIS for Terrain Modelling of the Georeferenced Raster Image. *Technologies* **2023**, *11*, 46. [CrossRef]
30. Gillies, S. Rasterio Documentation Release 1.5.0.dev. Available online: https://github.com/rasterio/rasterio (accessed on 26 February 2025).

https://doi.org/10.3390/app16073351